Crystal structure and near-infrared luminescence properties of novel binuclear erbium and erbium–ytterbium cocrystalline complexes†

Limei Song,[ab] Qi Wang,[ab] Daihua Tang,[a] Xinhou Liu[a] and Zhen Zhen*[a]

Received (in Montpellier, France) 10th November 2006, Accepted 4th January 2007
First published as an Advance Article on the web 2nd February 2007
DOI: 10.1039/b616422f

Three binuclear complexes of erbium and ytterbium, $Er_2(Ba)_6(Phen)_2$, $Yb_2(Ba)_6(Phen)_2$ and $Er_{1.4}Yb_{0.6}(Ba)_6(Phen)_2$ (Ba = benzoate, Phen = 1,10-phenanthroline), were synthesized and structurally characterized, and their luminescent properties examined in detail. Compared with the binuclear complex $Er_2(Ba)_6(Phen)_2$, the NIR luminescence of the erbium ion in $Er_{1.4}Yb_{0.6}(Ba)_6(Phen)_2$ is enhanced because of the coexistence of the ytterbium ion through an ytterbium-to-erbium energy transfer process. The full width at half maximum, centered at 1535 nm in the emission spectrum of $Er_{1.4}Yb_{0.6}(Ba)_6(Phen)_2$, is 108 nm, excited at 975 nm, which has potential to enable a wide-gain bandwidth for optical amplification. The X-ray single crystal structure confirms that this is an excellent binuclear complex model with a short metal-to-metal distance (about 4 Å) to facilitate the intramolecular (not intermolecular) Yb–Er energy transfer process. ESI-MS confirmed the molecules $Er_2(Ba)_6(Phen)_2$, $Yb_2(Ba)_6(Phen)_2$ and $ErYb(Ba)_6(Phen)_2$ exist in solution.

Introduction

To date, erbium-doped silica fiber amplifiers have been largely used in optical communication networks for signal amplification at a wavelength of around 1.54 μm. With the development of miniaturization and the integration of devices, organic optical amplification modules are more attractive because of their low costs, high packaging density and simple processing steps.[1–3] Generally, for erbium-doped organic optical amplification devices, it is better to embed the organic erbium complexes in an organic matrix due to the generally better solubility of organic complexes. So far, many erbium complexes for optical amplifiers have been discovered, mostly consisting of a central trivalent erbium ion and chelating ligands.[4–6] The ligands are designed to provide enough coordination sites to bind the central ion, to shield it from the surrounding matrix and also to act as "antenna chromophores" to transfer excitation energy to the encapsulated ion. In order to obtain stable lanthanide complexes with better optical properties, most investigations have focused on organic ligands such as diketones, quinolines, phenanthrolines, cryptands, *etc.*[7–11] Meanwhile, aromatic carboxylic acids, fluorine-containing compounds and heterocyclic ligands are also proving attractive owing to their high thermal and luminescent stabilities.[12–14]

However, the maximum absorption bands of organic ligands are usually in the ultraviolet or visible region and cannot utilize cheap commercial semiconductor LD as the excitation source. Direct excitation of the Er^{3+} ion at 980 nm is less efficient because of the intrinsically low absorption cross-section. As the absorption cross-section of Yb^{3+} at 980 nm is roughly ten times larger than that of Er^{3+},[15] the pump radiation at 980 nm can be efficiently absorbed and then transferred from the $^2F_{5/2}$ level of the Yb^{3+} to the $^4I_{11/2}$ level of the Er^{3+}. In this regard, a continuing challenge has been to develop and construct efficient functional systems to achieve Yb–Er energy transfer. In this paper we report the structure and near-infrared (NIR) luminescence properties of novel binuclear erbium and erbium–ytterbium co-crystalline complexes based on benzoate and 1,10-phenanthroline ligands. The 1,10-phenanthroline ligand chelated to an erbium ion acts as a light-harvesting moiety and sensitizer, which effectively transfers excitation energy to the erbium ion excited at 320 nm. Compared with $Er_2(Ba)_6(Phen)_2$, the NIR luminescence of the erbium ion in $Er_{1.4}Yb_{0.6}(Ba)_6(Phen)_2$ is enhanced, excited at both 320 and 975 nm, indicating an efficient energy transfer from Yb^{3+} to Er^{3+}.

Experimental

Materials and reagents

The solvents and reactants, including sodium benzoate, lanthanide chloride hydrates ($ErCl_3 \cdot 6H_2O$ and $YbCl_3 \cdot 6H_2O$) and hydrated 1,10-phenanthroline ($C_{12}H_8N_2 \cdot H_2O$), were analytical grade reagents and were used as received without further purification.

Physico-Chemical measurements

Elemental analysis was carried out with an Elementar Vario EL (Germany) analyzer. Thermogravimetric (TG) measurements were performed with a SDT Q600 analyzer with a heat

[a] *Technical Institute of Physics and Chemistry, Chinese Academy of Sciences, Beijing 100080, P. R. China. E-mail: zhenz@mail.ipc.ac.cn; Fax: +86 (10)62554670*
[b] *The Graduate University of Chinese Academy of Sciences, Beijing 100049, P. R. China*

† Electronic supplementary information (ESI) available: EDS data, calculated isotope patterns, NIR PL spectra and energy level diagram for the sensitization process. See DOI: 10.1039/b616422f

rate of 10 °C min^{-1} under a nitrogen atmosphere. The stoichiometry of erbium and ytterbium in $Er_{1.4}Yb_{0.6}(Ba)_6(Phen)_2$ was confirmed by EDS analysis using a HITACHI S-4300 scanning electron microscope. ESI-MS was performed with a QSTAR mass spectrometer, and samples used were small crystals. UV-vis spectra were measured with a U-2001 spectrophotometer. NIR steady state photoluminescence (NIR PL) spectra were recorded on an Edinburgh Instrument using an EI-germanium detector and a Xe lamp as the excitation source. The lifetime measurements at room temperature in the infrared region were performed on a Fluorolog FL3-11 spectrofluorimeter equipped with a SPEX 1934D phosphorimeter, monitoring the decay of the luminescence intensity excited at 975 nm. The decay signal arose 10 μs after excitation.

All the samples for photophysical measurements were obtained from their chloroform solutions. The solutions were stood for several days at room temperature and the solvent allowed to evaporate. The resulting microcrystalline powders were collected by pouring away the remaining liquid and dried *in vacuo*.

Syntheses

$Er_2(Ba)_6(Phen)_2$. A mixture of sodium benzoate (0.590 g, 4.094 mmol) and hydrated 1,10-phenanthroline ($C_{12}H_8N_2 \cdot H_2O$) (0.595 g, 3.002 mmol) was combined with THF (150 ml) to form a suspension. A solution of $ErCl_3 \cdot 6H_2O$ (0.521 g, 1.365 mmol) in methanol (10 ml) was added dropwise to the suspension. After stirring for 24 h at room temperature, the resulting mixture was filtered and solvents in the filtrate were removed under reduced pressure. The solid was washed with diethyl ether and n-hexane, and dried *in vacuo*. The obtained pink solid was dissolved in DMF, and the resulting solution stood at room temperature for more than one month. After this time, a single-crystal product suitable for X-ray analysis was collected by filtration. Calc. for $C_{66}H_{46}N_4O_{12}Er_2$: C, 55.76; H, 3.26; N, 3.94. Found: C, 55.63; H, 3.25; N, 3.94%.

$Er_{1.4}Yb_{0.6}(Ba)_6(Phen)_2$. A mixture of sodium benzoate (0.590 g, 4.094 mmol) and hydrated 1,10-phenanthroline ($C_{12}H_8N_2 \cdot H_2O$) (0.595 g, 3.002 mmol) was combined with THF (150 ml) to form a suspension. A solution of $ErCl_3 \cdot 6H_2O$ (0.365 g, 0.956 mmol) and $YbCl_3 \cdot 6H_2O$ (0.159 g, 0.410 mmol) in methanol (10 ml) was added dropwise to the suspension. After stirring for 24 h at room temperature, the resulting mixture was filtered and solvents in the filtrate were removed under reduced pressure. The solid was washed with diethyl ether and n-hexane, and dried *in vacuo*. Calc. for $C_{66}H_{46}N_4O_{12}Er_{1.4}Yb_{0.6}$: C, 55.58; H, 3.23; N, 3.93. Found: C, 55.61; H, 3.32; N, 3.85%.

$Yb_2(Ba)_6(Phen)_2$. A mixture of sodium benzoate (0.590 g, 4.094 mmol) and hydrated 1,10-phenanthroline ($C_{12}H_8N_2 \cdot H_2O$) (0.595 g, 3.002 mmol) was combined with THF (150 ml) to form a suspension. A solution of $YbCl_3 \cdot 6H_2O$ (0.529 g, 1.365 mmol) in methanol (10 ml) was added dropwise to the suspension. After stirring for 24 h at room temperature, the resulting mixture was filtered and solvents in the filtrate were removed under reduced pressure. The solid was washed with diethyl ether and n-hexane, and dried *in vacuo*. Calc. for $C_{66}H_{46}N_4O_{12}Yb_2$: C, 55.31; H, 3.24; N, 3.91. Found: C, 55.36; H, 3.27; N, 3.88%.

Table 1 Crystal data for $C_{66}H_{46}N_4O_{12}Er_2$

Empirical formula	$C_{66}H_{46}N_4O_{12}Er_2$
Temperature	296(2) K
Wavelength	0.71073 Å
Crystal system	Triclinic
Space group	*P*-1
Unit cell dimensions	a = 10.7122(9) Å
	b = 11.9131(10) Å
	c = 12.4072(10) Å
	α = 105.252(2)°
	β = 93.448(2)°
	γ = 113.481(2)°
Z	1
Absorption coefficient	3.099 mm^{-1}
$F(000)$	702
Crystal color and size	Pink, 0.3 × 0.2 × 0.2 mm^3
Reflections collected	13 274
Independent reflections	9706 (R_{int} = 0.0163)
Absorption correction	None
Refinement method	Full-matrix least-squares on F^2
Goodness-of-fit on F^2	1.049
R indices [$I > 2\sigma(I)$]	$R1^a$ = 0.0253, w$R2^b$ = 0.0650
R indices (all data)	$R1$ = 0.0281, w$R2$ = 0.0666

^{a} $R1 = \Sigma||F_o| - |F_c||/\Sigma|F_o|$. ^{b} w$R2 = \{\Sigma[w(F_o^2 - F_c^2)^2]/\Sigma[w(F_o^2)^2]\}^{\frac{1}{2}}$.

Crystallography

X-Ray data were collected on a Bruker SMART APEX-CCD diffractometer with Mo-K_α radiation (λ = 0.71037 Å) using a ω-scan technique in the range 2.17 to 33.51°. The structure was solved by direct methods and refined by full-matrix least-squares on all F^2 data using the SHELXTL program.[16] All non-hydrogen atoms were refined anisotropically, and hydrogen atoms were located by geometry and assigned with common isotropic displacement factors. The weighting scheme of the final refinement was achieved by the following formula: $w = 1/[\sigma^2(F_o)^2 + (0.0357P)^2 + 0.0779P]$, where $P = (F_o^2 + 2F_c^2)/3$. The final difference electron density map showed a highest peak of 1.752 e$Å^{-3}$, located 0.71 Å from Er(1), and a deepest hole of −0.712 e$Å^{-3}$, located 0.80 Å from Er(1). The crystallographic and refinement data are summarized in Table 1, and selected bond distances and angles are listed in Table 2.‡

Results and discussion

We have prepared three complexes, $Er_2(Ba)_6(Phen)_2$, $Yb_2(Ba)_6(Phen)_2$ and $Er_{1.4}Yb_{0.6}(Ba)_6(Phen)_2$ (Ba = benzoate, Phen = 1,10-phenanthroline), through a ligand exchange reaction. To prepare the $Er_{1.4}Yb_{0.6}(Ba)_6(Phen)_2$ complex, $ErCl_3 \cdot 6H_2O$ and $YbCl_3 \cdot 6H_2O$, in a stoichiometry of 7 : 3, were added to the reaction.

Characterization

The single crystal of complex $Er_2(Ba)_6(Phen)_2$ was verified by elementary analysis, TGA, X-ray diffraction analysis and ESI-MS. The crystals of complexes $Er_{1.4}Yb_{0.6}(Ba)_6(Phen)_2$ and $Yb_2(Ba)_6(Phen)_2$ were verified by elementary analysis and ESI-MS. The elementary analysis results matched well with

Table 2 Selected bond lengths (Å) and angles (°) for $C_{66}H_{46}N_4O_{12}Er_2$

Er–O(1)	2.3475(15)	O(6)–Er–O(2)	76.87(6)
Er–O(2)	2.4673(17)	O(3)–Er–O(2)	131.98(6)
Er–O(3)	2.3000(15)	O(5)–Er–O(2)	77.78(6)
Er–O(4)	2.3397(15)	O(4)–Er–O(2)	142.72(6)
Er–O(5)	2.3062(15)	O(1)–Er–O(2)	53.96(6)
Er–O(6)	2.2463(16)	O(6)–Er–N(1)	145.00(6)
Er–N(1)	2.5286(19)	O(3)–Er–N(1)	140.28(6)
Er–N(2)	2.5986(19)	O(5)–Er–N(1)	78.34(6)
O(6)–Er–O(3)	73.81(6)	O(4)–Er–N(1)	75.53(6)
O(6)–Er–O(5)	79.88(6)	O(1)–Er–N(1)	86.73(6)
O(3)–Er–O(5)	131.47(6)	O(2)–Er–N(1)	71.97(6)
O(6)–Er–O(4)	125.82(6)	O(6)–Er–N(2)	146.38(6)
O(3)–Er–O(4)	85.11(6)	O(3)–Er–N(2)	76.81(6)
O(5)–Er–O(4)	78.23(6)	O(5)–Er–N(2)	132.92(6)
O(6)–Er–O(1)	87.68(6)	O(4)–Er–N(2)	66.51(6)
O(3)–Er–O(1)	87.50(6)	O(1)–Er–N(2)	74.98(6)
O(5)–Er–O(1)	131.73(6)	O(2)–Er–N(2)	112.76(6)
O(4)–Er–O(1)	141.47(6)	N(1)–Er–N(2)	63.73(6)

theoretical values. The stoichiometry of erbium and ytterbium in $Er_{1.4}Yb_{0.6}(Ba)_6(Phen)_2$ was confirmed by EDS analysis, with atomic percentages of 13.98 and 5.78 for Er and Yb, respectively, which indicates a 7 : 3 molar ratio of Er to Yb (see Fig. S1 and Table S1 in the supplementary information†). As seen in Fig. 1, for complex $Er_2(Ba)_6(Phen)_2$, there is no obvious weight loss before 284 °C in the TGA curve, indicating that the complex has no coordinated water molecules. Two obvious weight loss processes are illustrated in the curve: the first process took place from 284 to 378 °C, assigned to the loss of Phen ligands, followed by a stage with the release of benzoate ligands until 577 °C.

Crystal structure

The X-ray single-crystal structure analysis of $Er_2(Ba)_6(Phen)_2$‡ revealed that one molecule consists of two Er^{3+}, six benzoate groups and two Phen molecules. As shown in Fig. 2, each of the two Er^{3+} is coordinated by two N atoms of one Phen and six O atoms of five benzoate groups to form an 8-coordinated polyhedron. We can see that the six benzoate groups are of two kinds, four of which play bridging roles linking the two Er^{3+} by their O atoms, and the remaining two are directly bound to each Er^{3+}, respectively. Also, the two neutral Phen molecules use their N atoms to chelate each Er^{3+}. The Er–Er distance in the molecule is 4.0675(4) Å. The mean value of the Er–O bond length is 2.3345 Å (varying from 2.2463(16) to 2.4673(17) Å). The average Er–N bond distance is 2.5636 Å and the N–Er–N bond angle is 63.73(6)° (Table 2). The relationship between the Er–N bond distances and the N–Er–N bond angle is in good agreement with the summary for [Ln(Phen)] fragments by Bellusci *et al.*[17] Recently, several complexes with the formula $Ln_2(Ba)_6(Phen)_2$ (Ln = La,[18] Sm,[19] Eu,[20] Gd[21] and Tb[22]) have been reported successively. All of them crystallize in space group *P*-1, which is accordant with the refinement of $Er_2(Ba)_6(Phen)_2$. It is reasonably assumed that the structure of the Yb–Er co-crystalline complex and that of $Yb_2(Ba)_6(Phen)_2$ are the same as for the erbium complex; both belonging to space group *P*-1.

‡ CCDC reference numbers 619673. For crystallographic data in CIF or other electronic format see DOI: 10.1039/b616422f

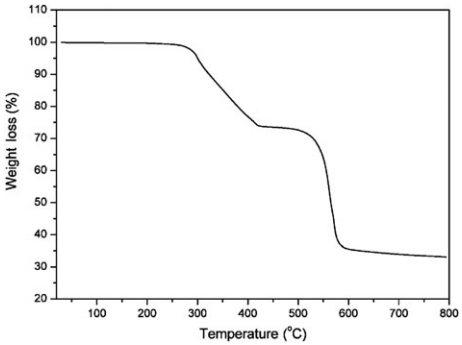

Fig. 1 TGA diagram of $[Er_2(Ba)_6(Phen)_2]$.

ESI-MS

The ESI-MS of the three binuclear complexes, $Er_2(Ba)_6(Phen)_2$, $Er_{1.4}Yb_{0.6}(Ba)_6(Phen)_2$ and $Yb_2(Ba)_6(Phen)_2$ (Fig. 3), confirm that each binuclear molecule exists in solution. The experimental and calculated isotope patterns are consistent with each other (see Fig. S2 in the supplementary information†). For $Er_{1.4}Yb_{0.6}(Ba)_6(Phen)_2$, two molecules, $Er_2(Ba)_6(Phen)_2$ and $ErYb(Ba)_6(Phen)_2$, are indicated in solution. The peak of $[Yb_2(Ba)_5(Phen)_2]^+$ is not clearly detectable, indicating almost no $Yb_2(Ba)_6(Phen)_2$ in the solution. The peak at m/z = 1305.3977 is clearly detectable, which is attributed to $[ErYb(Ba)_5(Phen)_2]^+$. According to the ESI-MS analysis, the $Er_{1.4}Yb_{0.6}(Ba)_6(Phen)_2$ complex probably consists of two kinds of molecule, $Er_2(Ba)_6(Phen)_2$ and $ErYb(Ba)_6(Phen)_2$, which co-crystallize in a particular ratio. Based on the stoichiometry of the lanthanide ions the $Er_{1.4}Yb_{0.6}(Ba)_6(Phen)_2$ complex may correspond to $2[Er_2(Ba)_6(Phen)_2] \cdot 3[ErYb(Ba)_6(Phen)_2]$. That is, for every two molecules of $Er_2(Ba)_6$

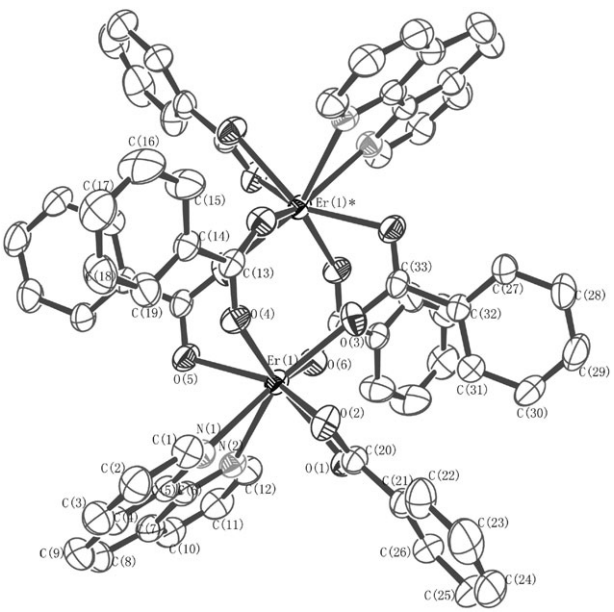

Fig. 2 The molecular structure of $C_{66}H_{46}N_4O_{12}Er_2$ (50% probability ellipsoids). The hydrogen atoms are omitted for clarity. The asterisk symbol indicates that this atom is at equivalent position (2 − *x*, 2 − *y*, 2 − *z*).

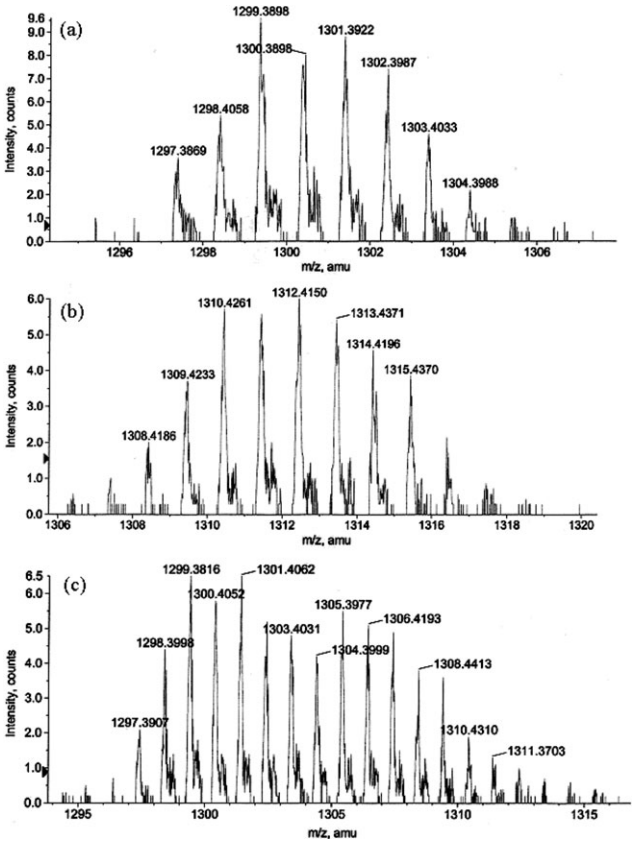

Fig. 3 Expanded regions of the ESI-MS of $Ln_2(Ba)_6(Phen)_2$ complexes in methanol. (a) Spectrum of $Er_2(Ba)_6(Phen)_2$, $[Er_2(Ba)_5(Phen)_2]^+$ m/z = 1297.142. (b) Spectrum of $Yb_2(Ba)_6(Phen)_2$, $[Yb_2(Ba)_5(Phen)_2]^+$ m/z = 1313.160. (c) Spectrum of $Er_{1.4}Yb_{0.6}(Ba)_6(Phen)_2$, $[ErYb(Ba)_5(Phen)_2]^+$ m/z = 1305.151.

$(Phen)_2$, there are three molecules of $ErYb(Ba)_6(Phen)_2$ co-crystallized with it.

Photophysical properties and energy transfer processes

The complexes formed when the molar ratio of $ErCl_3 \cdot 6H_2O$ to $YbCl_3 \cdot 6H_2O$ added to the reaction was 3 : 7 and 1 : 1, respectively were also synthesized. By investigating the NIR PL spectra of complexes $Er_{2-x}Yb_x(Ba)_6(Phen)_2$ (x = 0, 0.6, 1.0, 1.4 and 2.0) around 1535 nm, excited at 320 nm at room temperature (see Fig. S3 in the supporting information†), we found that $Er_{1.4}Yb_{0.6}(Ba)_6(Phen)_2$ had the strongest luminescence. Therefore, the emphasis of our studies has been on complex $Er_{1.4}Yb_{0.6}(Ba)_6(Phen)_2$.

The UV-vis absorption spectra of Phen, benzoic acid, $Er_2(Ba)_6(Phen)_2$, $Er_{1.4}Yb_{0.6}(Ba)_6(Phen)_2$ and $Yb_2(Ba)_6(Phen)_2$ are shown in Fig. 4. The absorption band of benzoic acid peaks at around 282 nm, while the absorption spectrum of Phen shows a broad intense absorption band around 320 nm due to a π–π* electronic transition. It is clear that the absorption spectra of all the complexes are similar to that of Phen, suggesting that the coordination of the lanthanide ions do not have a significant influence on the π–π* transition. Some weak peaks in the absorption spectra (at 380, 521 and 650 nm) of the $Er_2(Ba)_6(Phen)_2$ and $Er_{1.4}Yb_{0.6}(Ba)_6(Phen)_2$ complexes are

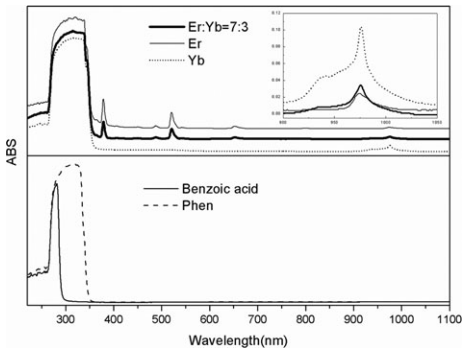

Fig. 4 Top: UV-Vis spectra of Er_2 $(Ba)_6(Phen)_2$, $Er_{1.4}Yb_{0.6}(Ba)_6(Phen)_2$ and $Yb_2(Ba)_6(Phen)_2$ (0.01M, DMF). Top inset: Absorption around 980 nm. Bottom: Absorption spectra of Phen and benzoic acid (0.01M, DMF).

attributed to the intrinsic absorption bands of Er^{3+}. The absorption bands around 980 nm, originating from Er^{3+} as well as Yb^{3+}, are also shown in the inset spectra, indicating the stronger absorption of Yb^{3+} compared to Er^{3+}.

The luminescence spectra of bulk microcrystalline powders of complexes $Er_2(Ba)_6(Phen)_2$, $Er_{1.4}Yb_{0.6}(Ba)_6(Phen)_2$ and $Yb_2(Ba)_6(Phen)_2$, upon optical excitation in the absorption band of Phen (320 nm), are shown in Fig. 5. The emission around 1000 nm, assigned to the $^2F_{5/2} \rightarrow {}^2F_{7/2}$ transition of Yb^{3+}, is observed in $Yb_2(Ba)_6(Phen)_2$, and the characteristic emission band around 1535 nm, assigned to the $^4I_{13/2} \rightarrow {}^4I_{15/2}$ transition of Er^{3+}, is also observed in $Er_2(Ba)_6(Phen)_2$. For $Er_{1.4}Yb_{0.6}(Ba)_6(Phen)_2$, the emission intensity around 1000 nm decreases significantly and the emission intensity around 1535 nm is enhanced. These results confirm that energy transfer processes do occur from Phen to Yb^{3+} (and Er^{3+}), as well as from Yb^{3+} to Er^{3+}. For the luminescence of Yb^{3+}, a sensitive mechanism, different from the antenna effect, is possible because the excited state $^2F_{5/2}$ of Yb^{3+} is about 10 235 cm^{-1}, eliminating any possible energy match with the Phen ligand singlet (S_1, *ca.* 3.87 ev, *viz.* 31 150 cm^{-1}) or triplet

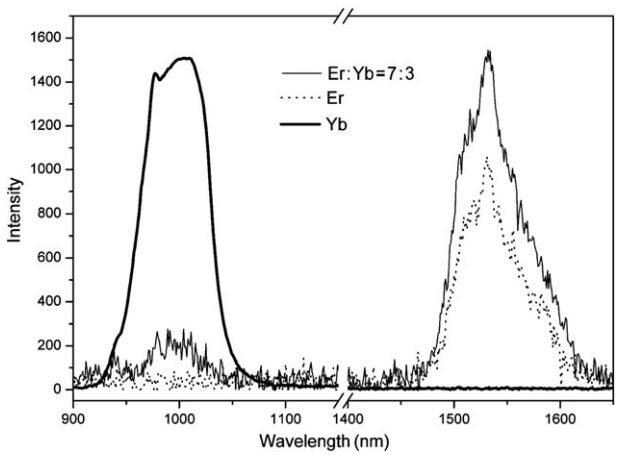

Fig. 5 NIR PL spectra of $Yb_2(Ba)_6(Phen)_2$ and $Er_{1.4}Yb_{0.6}(Ba)_6(Phen)_2$ around 1000 nm, and the NIR PL spectra of $Er_2(Ba)_6(Phen)_2$ and $Er_{1.4}Yb_{0.6}(Ba)_6(Phen)_2$ around 1535 nm. The bulk microcrystalline powders were excited at 320 nm at room temperature. The PL curve of $Yb_2(Ba)_6(Phen)_2$ is reduced by 15-fold.

(T_1, *ca.* 2.09 ev, *viz.* 16 823 cm^{-1}) levels.[23] Two main explanations for the energy mismatch luminescence have been reported.[24,25] One is an electron transfer mechanism involving a Yb^{3+}/Yb^{2+} redox couple: the initial reduction of Yb^{3+} by the ligand in its excited singlet state produces $(ligand)^{\cdot+}$–(Yb^{2+}) and the electron returning produces ligand–(Yb^{3+})*, resulting in the NIR luminescence of Yb^{3+}. The other is a phonon-assisted energy transfer process, which is a non-radiative relaxation process where the excess energy is transformed into vibrational energy and ultimately heat. In this explanation, it is considered that the lanthanide ion, with its ligands, forms one chromophore, and that non-radiative relaxation occurs from a higher excited state of the same chromophore rather than from the ligand to Yb^{3+}.

According to the generally accepted mechanism[26,27] and the photophysical properties of Phen complexes,[28,29] the photophysical pathway of the pure erbium complex $Er_2(Ba)_6(Phen)_2$ can be summarized as follows. The complex is first excited from the singlet S_0 ground state of Phen to its singlet S_1 excited state, followed by an intersystem crossing (ISC) from singlet state S_1 to triplet state T_1. Compared to the free ligand, this process is facilitated in a lanthanide complex because of spin–orbital coupling induced by heavy atom effects. Subsequently, energy transfer from the T_1 to the Er^{3+} 4f levels takes place. According to Dexter's theory,[30] the suitability of the energy difference between the resonance level of the Ln^{3+} ion and the triplet state of the ligand is a crucial factor for efficient energy transfer. If the energy difference is too large, the energy transfer rate constant will decrease due to the diminishing overlap between the donor and acceptor. On the other hand, if the energy difference is too small, energy back-transfer from the Ln^{3+} ion to the ligand will take place. In terms of the corresponding energy gap, the best-matching level of Er^{3+} might be the $^4F_{9/2}$ level. Next, the energy rapidly relaxes to the $^4I_{13/2}$ first excited state of the Er^{3+} ion, and finally the Er^{3+} ion may decay to $^4I_{15/2}$ ground manifold by emitting light (1535 nm).

Compared to $Er_2(Ba)_6(Phen)_2$, $Er_{1.4}Yb_{0.6}(Ba)_6(Phen)_2$ exhibits an enhanced luminescence intensity at 1535 nm because of the participation of Yb^{3+}. Meanwhile, compared to $Yb_2(Ba)_6(Phen)_2$, the luminescence intensity around 1000 nm in $Er_{1.4}Yb_{0.6}(Ba)_6(Phen)_2$ decreases considerably due to the co-crystallization of Er^{3+}. This confirms that Yb^{3+} contributes to the emission of Er^{3+}. The full widths at half maximum (FWHM) centered at 1535 nm in the emission spectra of $Er_{1.4}Yb_{0.6}(Ba)_6(Phen)_2$ and $Er_2(Ba)_6(Phen)_2$, excited at 320 nm, are 63 and 62 nm, respectively. From the above discussion of the energy mismatch luminescence of Yb^{3+}, the sensitive process of Er^{3+} in $Er_{1.4}Yb_{0.6}(Ba)_6(Phen)_2$ can be described as follows: Yb^{3+} is first sensitized *via* an electron transfer or phonon-assisted energy transfer process, and then most of the energy is transferred to the Er^{3+}.

Fig. 6 shows the NIR PL spectra of bulk microcrystalline powders of complexes $Er_{1.4}Yb_{0.6}(Ba)_6(Phen)_2$ and $Er_2(Ba)_6(Phen)_2$ around 1535 nm, excited at 975 nm. Compared to $Er_2(Ba)_6(Phen)_2$, $Er_{1.4}Yb_{0.6}(Ba)_6(Phen)_2$ exhibits a stronger emission due to the stronger absorption of Yb^{3+}. The Er^{3+} of $Er_{1.4}Yb_{0.6}(Ba)_6(Phen)_2$ is excited indirectly *via* an effective energy transfer from the energy level $^2F_{5/2}$ of Yb^{3+} to the $^4I_{11/2}$

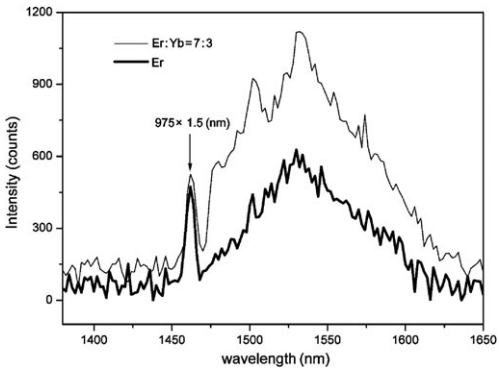

Fig. 6 NIR PL spectra of bulky microcrystalline powders of complexes $Er_{1.4}Yb_{0.6}(Ba)_6(Phen)_2$ and $Er_2(Ba)_6(Phen)_2$ around 1535 nm, excited at 975 nm at room temperature.

level of Er^{3+}, then rapidly relaxes to the $^4I_{13/2}$ level, and finally results in the emission around 1535 nm. To enable a wide-gain bandwidth for optical amplification, a broad emission band is desirable. For complex $Er_2(Ba)_6(Phen)_2$, the FWHM centered at 1535 nm is 75 nm in the emission spectra excited at 975 nm. It is noteworthy that the FWHM of $Er_{1.4}Yb_{0.6}(Ba)_6(Phen)_2$ centered at 1535 nm and excited at 975 nm is 108 nm. To our knowledge, this is an exceptionally broad emission band for an erbium-based organic complex excited at 975 nm. For instance, the FWHM for an Er(III) ion-association ternary complex with a NIR dye is 80 nm.[31] This indicates that the ytterbium ions contribute to the emission of the erbium ions.

A schematic drawing of the energy transfer process is shown in Fig. S4 of the supporting information.†

In the sensitive process of Er^{3+} luminescence by Yb^{3+}, the $Er^{3+}\cdots Yb^{3+}$ distances play significant roles. The shorter the $Er^{3+}\cdots Yb^{3+}$ distance, the more effective the sensitization. The X-ray single-crystal structure confirms that the intramolecular $Er^{3+}\cdots Er^{3+}$ distance is about 4 Å in $Er_2(Ba)_6(Phen)_2$. It is reasonably deduced that the intramolecular $Yb^{3+}\cdots Er^{3+}$ distance of $ErYb(Ba)_6(Phen)_2$ in $Er_{1.4}Yb_{0.6}(Ba)_6(Phen)_2$ is also about 4 Å, which facilitates the intramolecular (not intermolecular) Yb–Er energy transfer process.

Table 3 presents the radiative lifetimes (τ) of Er^{3+} and Yb^{3+} in $Er_2(Ba)_6(Phen)_2$, $Er_{1.4}Yb_{0.6}(Ba)_6(Phen)_2$ and $Yb_2(Ba)_6(Phen)_2$, measured at an excitation wavelength of 975 nm. The luminescence of the $^4I_{13/2}$ level of Er^{3+} was monitored at 1535 nm and the luminescence of Yb^{3+}, originating from the $^2F_{5/2}$ level, was monitored at 1020 nm. The lifetimes for Er^{3+} and Yb^{3+} were all in the μs range. These short lifetimes are probably ascribed to the luminescence quenching by a number of C–H groups.

Table 3 Luminescence decay times (τ) of $Ln_2(Ba)_6(Phen)_2$

Complex	Ln	Wavelength/nm	τ/μs
$Er_2(Ba)_6(Phen)_2$	Er	1535	17.7
$Er_{1.4}Yb_{0.6}(Ba)_6(Phen)_2$	Er	1535	19.3
$Er_{1.4}Yb_{0.6}(Ba)_6(Phen)_2$	Yb	1020	26.7
$Yb_2(Ba)_6(Phen)_2$	Yb	1020	58.9

Conclusions

In summary, novel Er–Yb co-crystalline complex $Er_{1.4}Yb_{0.6}(Ba)_6(Phen)_2$ exhibits sensitized NIR emission, with a luminescence lifetime in the μs range. Although the energy transfer process from the chromophores to rare earth metal ions is suggested by an antenna effect, in this case, Phen sensitizes Yb^{3+}, probably *via* an electron transfer or a phonon-assisted energy transfer process. The FWHM, centered at 1535 nm in the emission spectrum of $Er_{1.4}Yb_{0.6}(Ba)_6(Phen)_2$, is 108 nm, excited at 975 nm, which has the potential to enable a wide-gain bandwidth for optical amplification. The X-ray single-crystal structure confirms that this is an excellent binuclear complex model, with a short metal-to-metal distance (about 4 Å) that facilitates such an intramolecular (not intermolecular) Yb–Er energy transfer process.

Acknowledgements

We are grateful to the National Natural Science Foundation of China (no. 20374058) for financial support.

References

1 K. Kuriki and Y. Koike, *Chem. Rev.*, 2002, **102**, 2347.
2 L. H. Slooff, A. Van Blaaderen and A. Polman, *J. Appl. Phys.*, 2002, **91**, 3955.
3 W. H. Wong, E. Y. B. Pun and K. S. Chan, *Appl. Phys. Lett.*, 2004, **84**, 176.
4 B. O. Jae, H. K. Yong, K. N. Min and K. K. Hwan, *J. Lumin.*, 2005, **111**, 255.
5 S. Destri, W. Porzio, F. Meinardi, R. Tubino and G. Salerno, *Macromolecules*, 2003, **36**, 273.
6 M. Kawa and J. M. J. Fréchet, *Chem. Mater.*, 1998, **10**, 286.
7 R. B. Pode, *Phys. Status Solidi A*, 1998, **170**, 137.
8 H. Suzuki, Y. Hattori, T. Lizuka, K. Yuzawa and N. Matsumoto, *Thin Solid Films*, 2003, **39**, 288.
9 M. P. Oude Wolbers, F. C. J. M. van Veggel, B. H. M. Snellink-Ruël, J. W. Hofstraat, F. A. J. Geurts and D. N. Reinhoudt, *J. Am. Chem. Soc.*, 1997, **119**, 138.
10 F. Artizzu, P. Deplano, L. Marchió, M. L. Mercuri, L. Pillia, A. Serpe, F. Quochi, R. Orrù, F. Cordella, F. Meinardi, R. Tubino, A. Mura and G. Bongiovanni, *Inorg. Chem.*, 2005, **44**, 840.
11 L. N. Sun, H. J. Zhang, L. S. Fu, F. Y. Liu, Q. G. Meng, C. Y. Peng and J. B. Yu, *Adv. Funct. Mater.*, 2005, **15**, 1041.
12 S. G. Roh, M. K. Nah, J. B. Oh, N. S. Baek, K. M. Park and H. K. Kim, *Polyhedron*, 2005, **24**, 137.
13 Y. S. Song, B. Yan and Z. X. Chen, *J. Solid State Chem.*, 2004, **177**, 3805.
14 G. Mancino, A. J. Ferguson, A. Beeby, N. J. Long and T. S. Jones, *J. Am. Chem. Soc.*, 2005, **127**, 524.
15 C. Strohhöfer and A. Polman, *Opt. Mater.*, 2003, **21**, 705.
16 *SHELXTL: Structure Determination Program (Version 6.10)*, Bruker AXS Inc., Madison, Wisconsin, USA, 2001.
17 A. Bellusci, G. Barberio, A. Crispini, M. Ghedini, M. L. Deda and D. Pucci, *Inorg. Chem.*, 2005, **44**, 1818.
18 Q. Shi, M. L. Hu, R. Cao, Y. C. Liang and M. C. Hong, *Acta Crystallogr., Sect. E: Struct. Rep. Online*, 2001, **57**, m122.
19 S. Y. Niu, J. Jin, W. M. Bu, G. D. Yang, J. Q. Cao and B. Yang, *Jiegou Huaxue*, 1999, **18**, 245.
20 S. Y. Niu, B. Yang, J. Q. Cao, D. Y. Yang and W. M. Bu, *Gaodeng Xuexiao Huaxue Xuebao*, 1997, **12**, 1917.
21 S. Y. Niu, J. Jin, X. L. Jin and Z. Z. Yang, *Solid State Sci.*, 2002, **4**, 1103.
22 R. F. Wang, S. P. Wang, S. K. Shi and J. J. Zhang, *Jiegou Huaxue*, 2004, **23**, 1300.
23 H. Xin, M. Shi, X. C. Gao, Y. Y. Huang, Z. L. Gong, D. B. Nie, H. Cao, Z. Q. Bian, F. Y. Li and C. H. Huang, *J. Phys. Chem. B*, 2004, **108**, 10796.
24 W. D. Horrocks, Jr., J. P. Bolender, W. D. Smith and R. M. Supkowski, *J. Am. Chem. Soc.*, 1997, **119**, 5972.
25 C. Reinhard and H. U. Güdel, *Inorg. Chem.*, 2002, **41**, 1048.
26 L. H. Slooff, A. Polman, M. P. Oude Wolbers, F. C. J. M. Van Veggel, D. N. Reinhoudt and J. W. Hofstraat, *J. Appl. Phys.*, 1998, **83**, 497.
27 O. H. Park, S. Y. Seo, B. S. Bae and J. H. Shin, *Appl. Phys. Lett.*, 2003, **82**, 2787.
28 R. V. Deun, P. Nockemann, C. Görller-Walrand and K. Binnemans, *Chem. Phys. Lett.*, 2004, **397**, 447.
29 M. Flores, U. Caldiño and R. Arroyo, *Opt. Mater. (Amsterdam)*, 2006, **28**, 514.
30 D. L. Dexter, *J. Chem. Phys.*, 1953, **21**, 836.
31 H. S. Wang, G. D. Qian, M. Q. Wang, J. H. Zhang and Y. S. Luo, *J. Phys. Chem. B*, 2004, **108**, 8084.